DETERMINATION OF EDDY CURRENT EFFECTS ON RADIAL ACTIVE MAGNETIC BEARINGS BASED ON A RELUCTANCE NETWORK AND 1D EDDY CURRENT MODEL

Matti Antila,[1] Erkki Lantto,[1] Ville Tommila[1]

ABSTRACT

The emphasis of this paper is to study the effects of eddy currents in radial magnetic bearings on the control system design and bearing dynamics. We create a model based on a nonlinear reluctance network and one-dimensional eddy current formulation. The model is a linearised model. We describe the formulation of reluctance network field solution, calculation of the linearised parameters and the implementation of the eddy current model. Two types of measurements have been done. First, we compare the dynamic impedance measurements and secondly, the dynamic bearing force measurements based on acceleration sensors.

INTRODUCTION

When designing a control system for an active magnetic bearing system, a designer needs a dynamic model of the bearing actuators. Usually, this model is formed from the linearised parameters of the actuators. They are the current stiffness, position stiffness and dynamic inductance. These parameters can be estimated by several methods ([Imlach et al., 1991, Knight et al. 1992, Hsiao and Lee, 1994, Meeker and Maslen, 1996, Schmidt et al., 1996, Antila et al., 1998]).

Common to all the above methods is that they are based on the stationary field solution. They neglect the effects of eddy currents and hysteresis and the linearised parameters are all real valued. As these effects are usually neglected in the dynamic models the true behaviour of an AMB system deviates from the designed one. Previously, Zmood et. al. [Zmood et al. 1987] presented a simple expansion term into the current stiffness. This simple model effectively describes the qualitative nature of the eddy current effect in one coordinate dimension. Meeker and Maslen [Meeker and Maslen, 1996] extended this formulation into arbitrary order. As well, they derived the one- dimensional eddy current formulation into a form suitable for large networks. They also made impedance measurements over a large frequency range and compared the calculated impedance with the measured one. The calculations were done based on the complex reluctivity formulation. The agreement of the amplitudes was found to be good and the major phase effects are

[1]Helsinki University of Technology, Laboratory of Electromechanics, P.O. Box 3000, 02015 HUT, Finland.

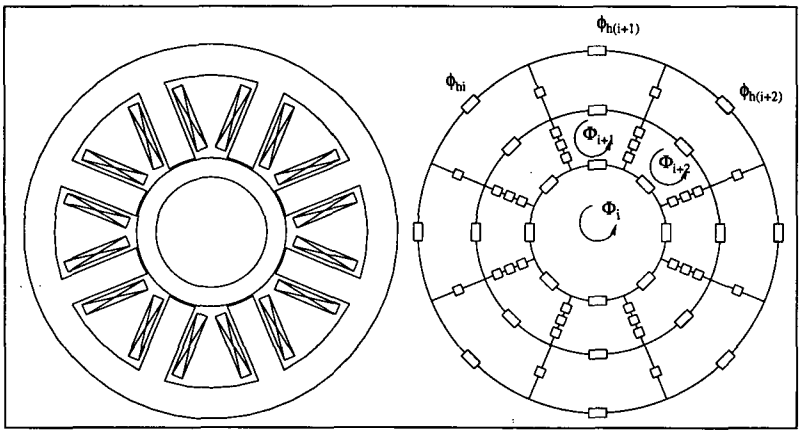

Figure 1: The geometry and reluctance network of an 8-pole radial active magnetic bearing.

at frequencies above 1000 Hz. However, the phase deviations around 1000 Hz were not clearly quantified.

In this work, we create a linearized state space model of a radial bearing including the eddy current effects. The model is based on the nonlinear reluctance network solution of the field and on the 1D eddy current model implemented into the reluctance network. The model is tested first by inductance measurements and by dynamic bearing force measurements based on acceleration sensors. These measurements and model estimations are used to study the phase errors at the particularly interesting frequency area from 50 to 3000 Hz.

RELUCTANCE NETWORK MODEL OF RADIAL AMB

In the reluctance network model, Maxwell's field equations are reduced to a set of magnetic circuit equations. The magnetic field distribution can be determined by solving a nonlinear and relatively small set of algebraic equations. The magnetic circuit is divided into reluctances the values of which depend on the geometry and the magnetisation of the material. It is worth to notice the assumptions used in the reluctance network model. The direction of the flux density is assumed to be known beforehand. The flux density is assumed to be constant on every flux carrying cross section. The leakage flux is assumed to flow only in the modelled leakage paths. The flux fringing in the vicinity of the airgap is taken into account by increasing the effective area of the airgap. The saturation of the magnetic circuit doesn't change the distribution of the magnetic field.

A typical geometry of an eight-pole radial magnetic bearing and its reluctance network model with loop fluxes are shown in Fig. 1. In this example, the stray flux between teeth is modelled with one stray flux reluctance and the reluctance of the tooth is divided into two parts. In the reluctance network model, we find the solution of the loop-fluxes shown in Fig. 1. The branch magnetic fluxes in the reluctances can be calculated from the loop-fluxes as follows

$$\boldsymbol{\phi}_\mathrm{h} = \mathbf{T}^T \boldsymbol{\Phi} \tag{1}$$

where $\mathbf{T}$ is the loop-set matrix, $\boldsymbol{\phi}_\mathrm{h}$ is a vector containing the branch fluxes and $\boldsymbol{\Phi}$ is a vector containing the loop-fluxes. The loop-set matrix $\mathbf{T}$ is formed as follows: $\mathrm{T}_{ij} = 1$, if branch j belongs to the route of loop flux i and the branch flux has the same direction as the loop flux. $\mathrm{T}_{ij} = -1$, if branch j belongs to the route of loop flux i and the branch flux has the opposite direction from the loop flux. $\mathrm{T}_{ij} = 0$, otherwise.

The same loop-set matrix connects also the loop-magnetomotive forces and the branch magnetomotive forces

$$\mathbf{T}\boldsymbol{f}_\mathrm{h} = \boldsymbol{M}_\mathrm{f} \tag{2}$$

where $\boldsymbol{M}_\mathrm{f}$ is a vector whose components are the loop-magnetomotive forces and vector $\boldsymbol{f}_\mathrm{h}$ contains the magnetomotive forces in the branch reluctances. The loop-magnetomotive force vector is calculated from coil currents and the number of coil turns per pole. The loop-magnetomotive vector entries are

$$\begin{aligned} \boldsymbol{M}_\mathrm{f} &= \boldsymbol{N}\boldsymbol{i} \\ \boldsymbol{i} &= [i_1 \cdots i_k]^T, \end{aligned} \tag{3}$$

where $\boldsymbol{i}$ is a vector of the coil currents and $\boldsymbol{N}$ is a coupling matrix, coupling the coil currents into magnetomotive forces of the loops. Thus, the entries of $\boldsymbol{M}_\mathrm{f}$ describe the total current flowing through the loop i. On the other hand, the magnetomotive forces and fluxes are connected to each other by diagonal reluctance matrix $\boldsymbol{R}_\mathrm{m}$

$$\begin{aligned} \boldsymbol{f}_\mathrm{h} &= \boldsymbol{R}_\mathrm{m}\boldsymbol{\phi}_\mathrm{h} \\ R_{mi} &= R_{mi}(\phi_{hi}), \end{aligned} \tag{4}$$

where R_mi is the reluctance of branch i. Due to the saturation of the core material the reluctance of branch i depends on the flux density and the geometry of the branch. The nonlinear magnetization curve is modelled by a single-valued monotonic reluctivity curve for the core material used. The values of the reluctances can be calculated from the geometry of the bearing.

The whole nonlinear system of equations can be expressed by the loop-fluxes and the loop-magnetomotive forces. This non-linear system is solved by Newton-Raphson iteration

$$\begin{aligned} \mathbf{T}\boldsymbol{R}_\mathrm{m}(\boldsymbol{\phi}_\mathrm{h})\,\mathbf{T}^T\boldsymbol{\Phi} &= \boldsymbol{M}_\mathrm{f} \\ &\Longrightarrow \\ \boldsymbol{r}^k &= \mathbf{T}\boldsymbol{R}_\mathrm{m}(\boldsymbol{\phi}_\mathrm{h}{}^k)\,\mathbf{T}^T\boldsymbol{\Phi}^k - \boldsymbol{M}_\mathrm{f}, \end{aligned} \tag{5}$$

where $\boldsymbol{r}(k)$ is the residual vector after k iteration steps. In the iteration process, the next values of the loop-fluxes are calculated from the previous values of residuals, loop-fluxes and Jacobian matrix $\boldsymbol{P}$.

$$\begin{aligned} \boldsymbol{\Phi}^{k+1} &= \boldsymbol{\Phi}^k - \boldsymbol{P}^{-1}\boldsymbol{r}^k \\ \boldsymbol{P}^k &= \mathbf{T}\frac{\partial(\boldsymbol{R}_\mathrm{m}(\boldsymbol{\phi}_\mathrm{h})\boldsymbol{\phi}_\mathrm{h})}{\partial\boldsymbol{\phi}_\mathrm{h}}\,\mathbf{T}^T. \end{aligned} \tag{6}$$

CALCULATION OF FORCES AND LINEARISED PARAMETERS

From the magnetic field solution, the static electromagnetic characteristics of a radial bearing can be derived. The force, current and position stiffness of the radial bearing is calculated based on the principle of virtual work.

$$W_m = \frac{1}{2}\int_0^{\boldsymbol{\Phi}} \boldsymbol{\Phi}^T \, \mathbf{T}\boldsymbol{R}_{\mathrm{m}} \, \mathbf{T}^T d\boldsymbol{\Phi} \tag{7}$$

$$\boldsymbol{F}_{\mathrm{b}} = -\frac{\partial W_m}{\partial \boldsymbol{p}}$$

$$\boldsymbol{F}_{\mathrm{b}} = -\frac{1}{2}\boldsymbol{\Phi}^T \, \mathbf{T}\frac{\partial \boldsymbol{R}_{\mathrm{m}}}{\partial \boldsymbol{p}} \, \mathbf{T}^T \boldsymbol{\Phi}, \tag{8}$$

where W_m is the magnetic energy of the system. The magnetic energy can be derived from the magnetic field solution and the derivative of the energy with respect to a virtual displacement $\boldsymbol{p}$ can be derived from the same solution It should be noticed that the partial differentiation with respect to the virtual displacement affects only the airgap reluctances. This means that the nonlinear energy integral of Eq. 7 reduces to a linear integral. Thus, implementation of this method is straightforward. The force can be calculated from the loop flux solution after the matrix $\frac{\partial \boldsymbol{R}_{\mathrm{m}}}{\partial \boldsymbol{p}}$ is formed.

In a similar fashion, the stiffness matrices and dynamic inductance matrix can be calculated from the magnetic field solution

$$\boldsymbol{h}_{\mathrm{f}} = -\frac{\partial^2 W_m}{\partial i \partial \boldsymbol{p}} = -\boldsymbol{\Phi}^T \, \mathbf{T}\frac{\partial \boldsymbol{R}_{\mathrm{m}}}{\partial \boldsymbol{p}} \, \mathbf{T}^T \boldsymbol{P}^{-1}\boldsymbol{N} \tag{9}$$

$$\boldsymbol{c} = -\frac{\partial^2 W_m}{\partial \boldsymbol{p} \partial \boldsymbol{p}} = -\boldsymbol{\Phi}^T \, \mathbf{T}\frac{\partial \boldsymbol{R}_{\mathrm{m}}}{\partial \boldsymbol{p}} \, \mathbf{T}^T \frac{\partial \boldsymbol{\Phi}}{\partial \boldsymbol{p}} \tag{10}$$

$$\boldsymbol{L}_{\mathrm{dyn}} = \frac{\partial \boldsymbol{\Psi}}{\partial \boldsymbol{i}} = \boldsymbol{N}^T \boldsymbol{P}^{-1}\boldsymbol{N}, \tag{11}$$

where $\boldsymbol{h}_{\mathrm{f}}$ is the current stiffness matrix, $\boldsymbol{c}$ is the position stiffness matrix, $\boldsymbol{L}_{\mathrm{dyn}}$ is the dynamic inductance matrix and $\boldsymbol{P}^{-1}$ is the inverse matrix of the Jacobian in Eq. 6 at the final iteration step. The derivative vector of the magnetomotive force with respect to coil current is as in Eq. 3. Thus, the matrices are calculated in one operation point.

THE EDDY CURRENT MODEL OF THE RADIAL AMB

In the previous section, the analysis based on the static magnetic field theory neglected the effect of eddy currents and hysteresis. The effect of eddy currents are analysed based on the one-dimensional eddy current model [Stoll, 1974, Meeker and Maslen, 1996]. This formulation is implemented into the reluctance network model of radial magnetic bearing. As a result, a linear model including the effect of eddy currents is produced. The nonlinearity of the magnetic circuit can be taken into account by linearising the system to the static operation point of the bearing.

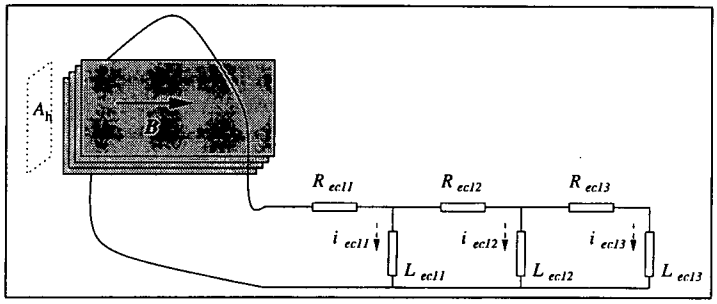

Figure 2: The interpretation of the eddy current model in one branch reluctance.

It is assumed that the material is homogenous, that is the reluctivity is constant inside the lamination. In a nonlinear analysis, the value of the reluctivity depends on the operation point of the bearing. Thus, the eddy current model can be seen as a small signal model in the neighbourhood of the operation point. At large amplitudes, the saturation along inside the lamination has a significant effect on the eddy current distribution and losses [Bottauscio et al., 1996]. It is worth to notice that this model describes only so called classical eddy current losses. This loss is due to the macroscopic conductivity of the iron sheet. Another equally important eddy current loss component usually called excess loss ([Saitz, 1997]) is neglected in this analysis. In practice, these loss components are of same magnitude, so this method is likely to underestimate the dynamic effects of eddy currents in AMB.

The model is a chain of inductances and resistances driven by a flux-changes in branch reluctances as shown in Fig. 2. The values of inductances and resistances are calculated from Eqs. 13, 14

$$\frac{i_{\mathrm{ec}}(s)}{\phi_{\mathrm{h}}(s)} = \frac{-s}{R_{\mathrm{ec1}} + \cfrac{1}{\cfrac{1}{sL_{\mathrm{ec1}}} + \cfrac{1}{R_{\mathrm{ec2}} + \cfrac{1}{\cfrac{1}{sL_{\mathrm{ec2}}} + \cdots}}}} \tag{12}$$

$$L_{\mathrm{ecj}} = \frac{A_{\mathrm{h}}\mu}{(4j+1)l} \tag{13}$$

$$R_{\mathrm{ecj}} = \frac{4(4j-1)A_{\mathrm{h}}}{\sigma l d^2}. \tag{14}$$

IMPLEMENTATION INTO THE RELUCTANCE NETWORK MODEL

The above model is possible to implement into the reluctance network model of radial magnetic bearings. As a result, we have a model of relatively low order (at least compared to 3-D FEM), and it is a linearized model. It can take into account both the saturation of the magnetic circuit and the eddy current effects. We present the model and associated linearised coupling matrices without detailed derivation.

$$\begin{aligned} \dot{\boldsymbol{X}}_{\mathrm{B}} &= \boldsymbol{A}_{\mathrm{B}}\boldsymbol{X}_{\mathrm{B}} + \boldsymbol{B}_{\mathrm{B}}\boldsymbol{U}_{\mathrm{B}} \\ \boldsymbol{Y}_{\mathrm{B}} &= \boldsymbol{C}_{\mathrm{B}}\boldsymbol{X}_{\mathrm{B}} + \boldsymbol{D}_{\mathrm{B}}\boldsymbol{U}_{\mathrm{B}} \end{aligned}$$

$$
\begin{aligned}
\boldsymbol{X}_\mathrm{B} &= [i_1 \cdots i_\mathrm{k}\ i_{\mathrm{ec11}} \cdots i_{\mathrm{ecl(order)}} \cdots i_{\mathrm{ecm1}} \cdots i_{\mathrm{ecm(order)}}\ \boldsymbol{p}^T]^T \\
\boldsymbol{Y}_\mathrm{B} &= [i_1 \cdots i_\mathrm{k}\ \boldsymbol{F}_\mathrm{B}^\mathrm{T}]^T \\
\boldsymbol{U}_\mathrm{B} &= [u_1 \cdots u_\mathrm{k}\ \dot{\boldsymbol{p}}^T]^T
\end{aligned}
$$

$$
\boldsymbol{A}_\mathrm{B} = \begin{bmatrix} -\boldsymbol{I}_\mathrm{B}\boldsymbol{R} & -\boldsymbol{I}_\mathrm{B}\boldsymbol{N}^T\boldsymbol{K}_3\ \mathrm{K_{tf2}}\boldsymbol{I}_\mathrm{A}\boldsymbol{R}_\mathrm{ec} & \boldsymbol{0} \\ -\boldsymbol{I}_\mathrm{A}\ \mathrm{K_{tf1}}\ \mathrm{T}^T\boldsymbol{K}_1\boldsymbol{I}_\mathrm{B}\boldsymbol{R} & -\boldsymbol{I}_\mathrm{A}\boldsymbol{R}_\mathrm{ec} - \boldsymbol{I}_\mathrm{A}\ \mathrm{K_{tf1}}\boldsymbol{T}^T\boldsymbol{K}_1\boldsymbol{I}_\mathrm{B}\boldsymbol{N}^T\boldsymbol{K}_3\ \mathrm{K_{tf2}}\boldsymbol{I}_\mathrm{A}\boldsymbol{R}_\mathrm{ec} & \boldsymbol{0} \\ \boldsymbol{0} & \boldsymbol{0} & \boldsymbol{0} \end{bmatrix} \tag{15}
$$

$$
\boldsymbol{B}_\mathrm{B} = \begin{bmatrix} \boldsymbol{I}_\mathrm{B} & \boldsymbol{I}_\mathrm{B}(\boldsymbol{h}_\mathrm{f}{}^T - \boldsymbol{N}^T\boldsymbol{K}_3\ \mathrm{K_{tf2}}\boldsymbol{I}_\mathrm{A}\ \mathrm{K_{tf1}}\ \mathrm{T}^T\boldsymbol{K}_2) \\ \boldsymbol{I}_\mathrm{A}\ \mathrm{K_{tf1}}\ \mathrm{T}^T\boldsymbol{K}_1\boldsymbol{I}_\mathrm{B} & \boldsymbol{I}_\mathrm{A}\ \mathrm{K_{tf1}}\ \mathrm{T}^T\boldsymbol{K}_1\boldsymbol{I}_\mathrm{B}(\boldsymbol{h}_\mathrm{f}{}^T - \boldsymbol{N}^T\boldsymbol{K}_3\ \mathrm{K_{tf2}}\boldsymbol{I}_\mathrm{A}\ \mathrm{K_{tf1}}\ \mathrm{T}^T\boldsymbol{K}_2) \\ \boldsymbol{0} & \boldsymbol{I} \end{bmatrix} \tag{16}
$$

$$
\boldsymbol{C}_\mathrm{B} = \begin{bmatrix} \boldsymbol{I} & \boldsymbol{0} & \boldsymbol{0} \\ \boldsymbol{h}_\mathrm{f} & \boldsymbol{h}_{\boldsymbol{i}_\mathrm{ecfe}} & \boldsymbol{c} \end{bmatrix} \tag{17}
$$

$$
\boldsymbol{I}_\mathrm{A} = [\boldsymbol{L}_\mathrm{ec} + \mathrm{K_{tf1}}\,\boldsymbol{T}^T\boldsymbol{K}_3\ \mathrm{K_{tf2}}]^{-1} \tag{18}
$$

$$
\boldsymbol{I}_\mathrm{B} = [\boldsymbol{L}_\mathrm{dyn} - \boldsymbol{N}^T\boldsymbol{K}_3\ \mathrm{K_{tf2}}\boldsymbol{I}_\mathrm{A}\ \mathrm{K_{tf1}}\ \mathrm{T}^T\boldsymbol{K}_1]^{-1} \tag{19}
$$

$$
\boldsymbol{h}_{\boldsymbol{i}_\mathrm{ecfe}} = \boldsymbol{\Phi}^T\ \mathrm{T}\frac{\partial \boldsymbol{R}_\mathrm{m}}{\partial \boldsymbol{p}}\ \mathrm{T}^T\boldsymbol{P}^{-1}\ \mathrm{T}\ \mathrm{K_{tf2}}. \tag{20}
$$

The transformation matrices used above are

$$
\boldsymbol{K}_1 = \frac{\partial \boldsymbol{\Phi}}{\partial \boldsymbol{i}} = \boldsymbol{P}^{-1}\frac{\partial \boldsymbol{M}_\mathrm{f}}{\partial \boldsymbol{i}} = \boldsymbol{P}^{-1}\boldsymbol{N} \tag{21}
$$

$$
\boldsymbol{K}_2 = \frac{\partial \boldsymbol{\Phi}}{\partial \boldsymbol{p}} \tag{22}
$$

$$
\boldsymbol{K}_3 = \frac{\partial \boldsymbol{\Phi}}{\partial \boldsymbol{i}_\mathrm{ec}} = \boldsymbol{P}^{-1}\frac{\partial \boldsymbol{M}_\mathrm{f}}{\partial \boldsymbol{i}_\mathrm{ec}} = \boldsymbol{P}^{-1}\ \mathrm{T} \tag{23}
$$

$$
\boldsymbol{\phi}_\mathrm{hfe} = \mathrm{K_{tf1}}\boldsymbol{\phi}_\mathrm{h} \tag{24}
$$

$$
\boldsymbol{i}_\mathrm{ec} = \mathrm{K_{tf2}}\boldsymbol{i}_\mathrm{ecfe}, \tag{25}
$$

where the notation is the same as in the previous section. It should be noticed that in Eq. 23 the partial differentiation is presented as if eddy currents would flow in all the branch reluctances. However, it is obvious that e.g. in the airgap reluctances no eddy currents exist. The vectors associated with the eddy currents are

$$
\frac{d\boldsymbol{\phi}_\mathrm{hfe}}{dt} = \boldsymbol{L}_\mathrm{ec}\frac{d\boldsymbol{i}_\mathrm{ecfe}}{dt} + \boldsymbol{R}_\mathrm{ec}\boldsymbol{i}_\mathrm{ecfe} \tag{26}
$$

$$
\boldsymbol{\phi}_\mathrm{hfe} = [\phi_{\mathrm{hf1}} \overbrace{0 \cdots 0}^{order-1}\ \phi_{\mathrm{hf2}} \overbrace{0 \cdots 0}^{order-1} \cdots \phi_{\mathrm{hfm}} \overbrace{0 \cdots 0}^{order-1}]^T \tag{27}
$$

$$
\boldsymbol{i}_\mathrm{ecfe} = [i_{\mathrm{ec11}}\ i_{\mathrm{ec12}} \cdots i_{\mathrm{ec1order}} \cdots i_{\mathrm{ecm1}}\ i_{\mathrm{ecm2}} \cdots i_{\mathrm{ecmorder}}]^T \tag{28}
$$

$$
\boldsymbol{i}_\mathrm{ec} = \left[\sum_{j=1}^{order} i_{\mathrm{ec1j}}\ \sum_{j=1}^{order} i_{\mathrm{ec2j}} \cdots 0\,0\,0 \cdots \sum_{j=1}^{order} i_{\mathrm{ecmj}} \cdots 0\,0 \cdots\right]^T, \tag{29}
$$

where $\boldsymbol{\phi}_\mathrm{hfe}$ is a modified branch flux vector, where $\boldsymbol{\phi}_\mathrm{hf}$ are only those branch reluctances where eddy currents exist. The $\boldsymbol{i}_\mathrm{ecfe}$ is the vector of the eddy currents in the model and

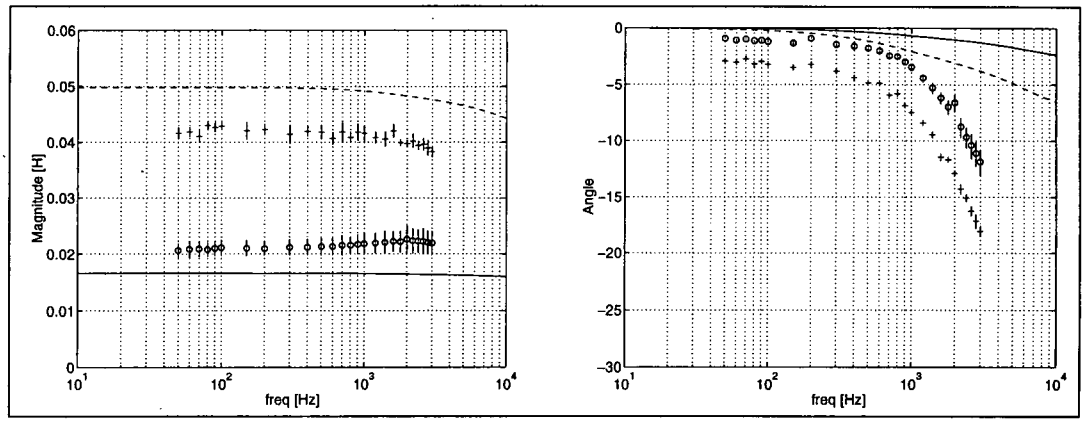

Figure 3: The dynamic inductance as a function of the frequency. The '+' and 'o' are the measurements at smaller (0.216 mm) and larger airgap (0.884 mm), respectively. The dashed and solid line are the calculated values correspondingly.

corresponds to the currents flowing through the inductors in Fig. 2. The $\boldsymbol{i}_{\mathrm{ec}}$ is a vector of size n, thus an element for every branch (also for airgap elements). Order is the number of the inductor-resistor pairs of the model used and n is the total number of branch reluctances of the model and m is the number of iron branch reluctances. The entries of the matrices $\boldsymbol{L}_{\mathrm{ec}}$ and $\boldsymbol{R}_{\mathrm{ec}}$ are calculated from Eqs. 13, 14.

EXPERIMENTS

IMPEDANCE MEASUREMENT

As a first indication of the validity of the eddy current model we measured the dynamic inductance at two different airgaps. The measurements were done with the high-speed compressor [Antila et al. 1996]. In Fig. 3 the dynamic inductance of the test machine is presented. The impedance is measured at two airgap values. The *DC*-current was in both measurements 0.25 A. This correspond to the airgap field of 0.15 T in the smaller airgap. Thus, both the measurements were done in the linear region.

The measured phase deviates from the calculated values. At lower frequencies, this is obvious because the hysteresis in the magnetic circuit is the dominant effect causing the phase lag. At higher frequencies, the main effect are caused by the eddy currents. As was already mentioned the excess loss component, which has a significant effect, was totally neglected in the analysis. The excess loss would roughly double the eddy current effect, so it is obvious that the deviation of the measured and calculated phases is not only because we neglected the excess loss. Anyhow, it can be seen that the deviation of the phase from the pure inductance is larger with smaller airgap. This is due to the fact that with smaller airgap the iron part of the circuit plays a greater role.

DYNAMIC FORCE MEASUREMENT

As a second measurement the dependence of the bearing force from the coil current was measured. The measurement was done by supplying disturbance at several frequencies

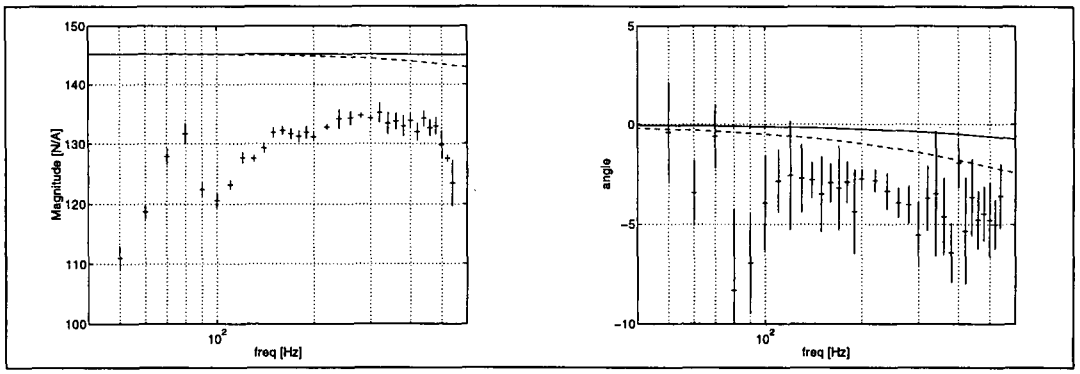

Figure 4: The current stiffness as a function of the frequency. The measured values are labeled with '+'. The solid line is the estimate based on the eddy current model. The dashed line is the eddy current estimate at double lamination thickness.

to the controller output and measuring the acceleration of the rotor at both ends of the rotor. Thus, the bearing forces could be calculated. The amplitude of the current at lower frequencies was chosen to be the same as the bias current, that is 2.0 A. The bearing force was calculated based on the modal reduced finite element rotor model [Lantto, 1997] The model for magnetic bearing force is the familiar one dimensional form

$$F_{\mathrm{bD}} = h_{\mathrm{fD}} i_{\mathrm{cD}} + c_{\mathrm{D}} x_{\mathrm{D}}, \tag{30}$$

where the quantities are at the D-end of the rotor. The primary interest is the current stiffness. The position stiffness was estimated from the measurements by least square method. The current stiffness was then calculated from Eq. 30. In the Fig. 4, comparison between the measured and calculated current stiffnesses are presented. At low frequencies, the measured magnitude decreases. This is purely calculational phenomenom as the position stiffness in Eq. 30 is estimated by one constant value. However, at smaller frequencies the vibration amplitudes are considerable with respect to airgap. So, the approximation of the position stiffness with one constant value is not valid at low frequencies. The agreement between measured and calculated phases is low. The fact that we neglected the excess loss explains some of the discrepancy. The deviation is larger at higher frequencies and could be caused by some additional unmodelled eddy current paths or the assumptions of the model. These are discussed in the conclusions. We have also plotted the calculated current stiffness at the double lamination thickness. This is purely to demonstrate the magnitude of the phase deviation. Anyhow, the important detail to consider is the phase lag of about five degree between the measured current and bearing force.

When designing the control system one would like to know the maximum phase lag these effects cause in realistic operation points. Based on the model we briefly study, how the magnitude and phase lag depend on the operation point. The relative current stiffness h_{frel} as a function of the bearing force is presented in Fig. 5. The control current varies from 0 to 5.8 A. The calculated values are at frequencies 100, 300, 500, 700, 1000

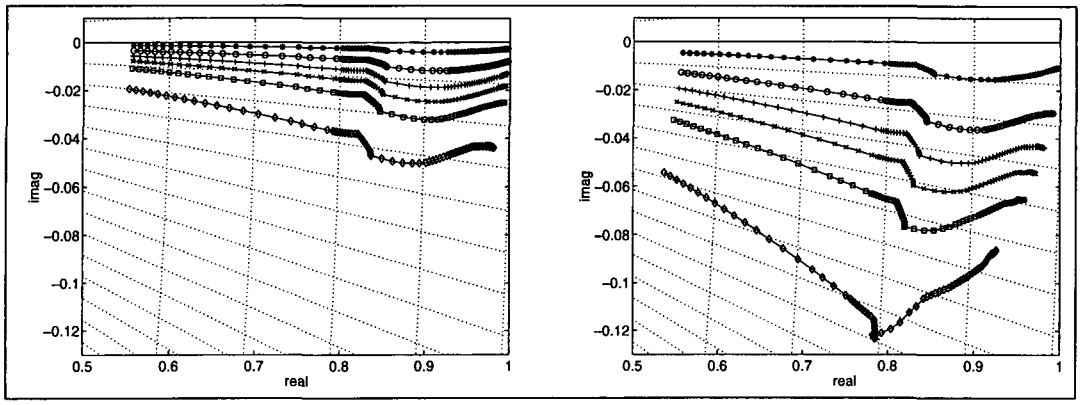

Figure 5: Calculated relative current stiffness h_{frel} as a function of the bearing force. The current stiffness is $h_{\text{f}} = h_{\text{frel}}$x145 N/A. Left, lamination thickness is 0.5 mm. Right, lamination thickness is 1.0 mm.

and 2000 Hz. The calculations are done with the lamination thickness of 0.5 mm and 1.0 mm. The calculated values are relative to the zero frequency current stiffness of 145 N/A. The saturation of the magnetic circuit is the major effect causing magnitude variations. The eddy currents are of minor importance in this respect. However, the phase lag due to eddy currents increases as a function of the bearing force until the maximum is found. This maximum is about 50 % higher than in the nominal point.

CONCLUSIONS

The eddy currents have a small effect on the magnitudes of the linearised parameters. However, the saturation of the magnetic circuit is the primary reasons for the variation of the magnitudes. At higher frequencies the agreement of the phase is not good. A part of this discrepancy is explained by the fact that we neglected the excess losses. The extra deviation can be mainly from two sources. First, the model is inadequate to describe the eddy current effects. The main assumption is the flux density profile inside the lamination [Meeker and Maslen, 1996]. The formula neglects the saturation in the lamination. At higher frequencies saturation is to happen near the surface of the sheet. In our impedance measurement the AC-component was same size as the DC-component. Thus, even at smaller airgap saturation is unlikely. The saturation could cause an unmodeled phase lag of few degrees. Anyhow at larger airgap, the flux density should remain well below saturation and no additional phase lag due to saturation should occur. In current stiffness measurement the current and flux density amplitudes are larger. For that reason, the saturation inside the lamination are likely to happen. A decrement in current stiffness above 500 Hz can be seen. This can be the effect of the saturation at the surface of the lamination.

Secondly, in the machine there are a lot of sources of unmodeled eddy current paths. One is at the rotor surface where the sheets may have small short circuit paths due to the machining of the rotor. Another one is the interlaminate currents due to inhomogeneities in the isolation and the high pressure when the sheets are stacked. These phenomena is of course stochastic by nature and difficult to model. In Fig. 4 it is presented also

calculation with double lamination thickness. Qualitatively the effect is the same as the interlaminate currents, of course quantitatively nothing can be said.

Thus, one can conclude that the accurate modelling of eddy currents is difficult. But for practical point of view one can conclude some guidelines for an AMB control system designer. In Fig. 3, it was clearly seen that the airgap has a large effect on the phase lag. For the controller point of view the worst case is if the rotor is eccentric and a bearing load is applied in the direction of eccentricity. Then on the other hand the phase lag is large and on the other hand the gain of the system is increased as the current stiffness is large. Thus, the phase margin decreases and at same time the crossover frequency increases. The crossover frequency is typically around 100-200 Hz. By considering the measurements and the results of the calculation, the additional phase lag due to hysteresis and eddy currents at the cross over frequency area is up to seven degree.

References

[Antila et al. 1996] Antila M., Lantto E., Saari J., Esa H., Lindgren O., Saily K. 1996. "Design of Water Treatment Compressors Equipped with Active Magnetic Bearings," *Proceedings of the Fifth International Symposium on Magnetic Bearings*, pp. 259-264, Kanazawa, Japan.

[Antila et al., 1998] Antila M., Lantto E., Arkkio A. 1998. "Determination of Forces and Linearised Parameters of Radial Active Magnetic Bearings by Finite Element Technique," accepted to be published in *IEEE Transactions on Magnetics.*

[Bottauscio et al., 1996] Bottauscio O., Chiampi M., Repetto M. 1996."Finite Element Analysis of Iron Loss Behaviour: Effect of Frequency and Lamination Thickness," *Proceedings of the 3rd International Workshop on Electric and Magnetic Fields*, pp. 417-422, Liege, Belgium.

[Hsiao and Lee, 1994] Hsiao F.-Z., Lee A.-C. 1994. "An investigation of the characteristic of electromagnetic bearings using the finite element method," *Transaction of the ASME Journal of Tribology*, 116:710-719.

[Imlach et al., 1991] Imlach J., Blair B.J., Allaire P. 1991. "Measured and predicted force and stiffness characteristic of industrial magnetic bearings," *Transaction of the ASME Journal of Tribology*, 113:784-788.

[Knight et al. 1992] Knight J., Xia Z., McCaul E., Hacker H.Jr. 1992. "Determination of forces in a magnetic bearing actuator: Numerical computation with comparison to experiment," *Transaction of the ASME Journal of Tribology*, 114:796-801.

[Lantto, 1997] Lantto E. 1997. "Finite Element Model for Elastic Rotating Shaft," *Acta Polytechnica Scandinavica.* Electrical Engineering Series No. 88.

[Meeker and Maslen, 1996] D.C. Meeker, Maslen E.H. 1996. "Augmented Circuit Model for Magnetic Bearings Including Eddy Currents, Fringing and Leakage," *IEEE Transactions on Magnetics*, 32(4):3219-3227.

[Saitz, 1997] J. Saitz. 1997. "Calculation of iron losses in electrical machines," Report 51, 57p., Espoo, Finland, Helsinki University of Technology, Laboratory of Electromechanics.

[Schmidt et al., 1996] E. Schmidt, T. Platter, H. Springer. 1996. "Force and Stiffness Calculations in Magnetic Bearings-Comparison between Finite Element Method and Network Theory," *Proceedings of the Fifth International Symposium on Magnetic Bearings*, pp. 259-264, Kanazawa, Japan.

[Stoll, 1974] Stoll R.L. 1974. "The Analysis of Eddy Currents," London:Oxford University Press.

[Zmood et al. 1987] Zmood R.B., Anand D.K., Kirk J.A. 1987. "The influence of Eddy Currents on Magnetic Actuator Perfomance," *Proc. IEEE*, 75:259-260.